Estimation of Sideslip and Roll Angles of Electric Vehicles Using Lateral Tire Force Sensors Through RLS and Kalman Filter Approaches

Kanghyun Nam, *Student Member, IEEE,* Sehoon Oh, *Member, IEEE,* Hiroshi Fujimoto, *Member, IEEE,* and Yoichi Hori, *Fellow, IEEE*

***Abstract*—Robust estimation of vehicle states (e.g., vehicle sideslip angle and roll angle) is essential for vehicle stability control applications such as yaw stability control and roll stability control. This paper proposes novel methods for estimating sideslip angle and roll angle using real-time lateral tire force measurements, obtained from the multi-sensing hub (MSHub) units, for practical applications to vehicle control systems of in-wheel-motor-driven electric vehicles. In vehicle sideslip estimation, a recursive least squares (RLS) algorithm with a forgetting factor is utilized based on a linear vehicle model and sensor measurements. In roll angle estimation, the Kalman filter is designed by integrating available sensor measurements and roll dynamics. The proposed estimation methods, RLS-based sideslip angle estimator and the Kalman filter are evaluated through field tests on an experimental electric vehicle. The experimental results show that the proposed estimator can accurately estimate the vehicle sideslip angle and roll angle. It is experimentally confirmed that the estimation accuracy is improved by more than 50% comparing to conventional method's one (see RMS error shown in Fig. 4). Moreover, the feasibility of practical applications of the lateral tire force sensors to vehicle state estimation is verified through various test results.**

***Index Terms*—Electric vehicles, Kalman filter, multi-sensing hub (MSHub) unit, recursive least squares (RLS), roll angle, sideslip angle.**

I. Introduction

DUE to the increasing concerns about advanced motion control of electric vehicles with in-wheel motors, a great deal of research on dynamics control for electric vehicles has been carried out [1]–[6]. Advanced motion control systems for electric vehicles, slip prevention, spinout prevention, and excessive roll prevention, are referred to as yaw stability control and roll stability control, respectively. Compared with internal combustion engine vehicles, electric vehicles with in-wheel motors have several advantages in the viewpoint of motion control [1], [3].

Manuscript received May 10, 2011; revised November 23, 2011; accepted for publication January 27, 2012. This work was supported in part by the Industrial Technology Research Grant Program from New Energy and Industrial Technology Development Organization (NEDO) of Japan.

K. Nam and S. Oh are with the Department of Electrical Engineering, Graduate School of Engineering, The University of Tokyo, Tokyo 113-8656, Japan (e-mail:nam@hori.k.u-tokyo.ac.jp; sehoon@hori.k.u-tokyo.ac.jp).

H. Fujimoto and Y. Hori are with the Department of Advanced Energy, Graduate School of Frontier Sciences, The University of Tokyo, Chiba 277-8561, Japan (e-mail:fujimoto@k.u-tokyo.ac.jp; hori@k.u-tokyo.ac.jp).

1) The torque generation of driving motors is very fast and accurate.
2) The driving torque can be easily measured from motor current.
3) Each wheel with an in-wheel motor can be independently controlled.

Based on these advantages, a novel yaw moment control method based on the yaw moment observer (YMO) was proposed in [7] and roll stability control for safety and driver's ride quality was proposed and verified with experimental results [8]. In most vehicle stability control systems, only a direct yaw rate feedback is used for improving the stability performances. However, on slippery road surfaces, controlling the vehicle sideslip angle to prevent it from becoming too large is also beneficial [9], [33].

Since the goal of aforementioned stability control systems is to control yaw rate, vehicle sideslip angle and roll angle, sensor measurements of yaw rate, vehicle sideslip angle, and roll angle are required. Yaw rate is easily measured by a cheap gyro sensor. However, since sensors for vehicle sideslip angle and roll angle are expensive, these must be estimated from available measurements and vehicle models. For this reason, a variety of estimation methods for estimating vehicle sideslip angle have been studied extensively [10]–[14]. Estimation methods based on state observers and Kalman filter design using a linear vehicle model were proposed and experimentally validated [15], [16]. Since linear vehicle model-based methods use constant vehicle and tire parameters, this method is not robust against parameter variations by changes in tire road conditions and driving conditions. In [17], the body slip angle fuzzy observer was proposed to deal with the nonlinearities in a vehicle model by representing the nonlinear models as Takagi-Sugeno (T–S) fuzzy models. In [18] and [19], nonlinear techniques for estimating lateral tire forces and sideslip angle, using extended and unscented Kalman filters, were proposed and evaluated by field tests. In [18], especially, the estimation method using nonlinear models shows the practical potential as a low-cost solution for calculating lateral tire forces and sideslip angle in real-time. In [20], [21], an adaptive sideslip angle observer considering tire-road friction adaptation (e.g., adaptation algorithm was designed using lateral vehicle dynamics) was proposed. A new methodology of combining a vehicle model-based method and a kinematics-based method was proposed and evaluated by experiments [11], [15]. Moreover, several researchers have

proposed new estimation methods using Global Positioning System (GPS) and inertial measurements to estimate vehicle sideslip angle without knowing the vehicle model [22], [28].

Over the last few years, several estimation methods were proposed to estimate roll states based on vehicle dynamics models without using additional sensors (e.g., roll rate sensor) [23]–[25]. In [25], several methods for roll angle estimation were discussed based on advantages and drawbacks of each method. Moreover, an approach using closed loop adaptive observer for roll angle and roll rate estimation was proposed and evaluated. In [23], a road-disturbance decoupled roll state estimator was designed, by combining the lateral model-based estimation method and vertical model-based estimation method, and evaluated by computer simulations. In other approaches [26]–[28], GPS with two laterally placed GPS antennas was used to estimate roll angle. GPS-based estimation approaches require satellite visibility from any location. However, the satellite visibility may be lost periodically in urban and forested driving environments and it causes inaccurate estimation. Even though GPS provides relatively accurate roll angle estimates under limited driving environments, it has a difficulty in vehicle applications due to the additional sensor cost.

In this paper, novel estimation methods based on lateral tire forces, measured by multi-sensing hub (MSHub) units [36], are proposed to provide accurate estimates of vehicle sideslip angle and roll angle. The recursive least squares (RLS) algorithm with a forgetting factor, which has been extensively utilized in the time-varying system identification [29], [34], was used to estimate lateral vehicle velocity for calculating sideslip angle. For estimating roll angle, the Kalman filter [35] was designed by using available sensor measurements and lateral vehicle velocity estimated from RLS. Kalman filter applications in vehicle state estimations have been widely discussed in the literature [14], [18], [30], and [31]. In order to make the best use of the advantages of in-wheel-motor-driven electric vehicles, it is necessarily required to accurately estimate the unmeasurable states using cost-effective sensors. At this point, this study presents the practical potential of MSHub units as a cost-effective solution for estimating vehicle states, which can improve the performance of vehicle control systems for in-wheel-motor-driven electric vehicles.

This paper is organized as follows. The vehicle model for estimator design is introduced in Section II. The conventional methods for estimating the vehicle sideslip angle are reviewed and a novel estimation method using MSHub units is proposed and evaluated by experiments in Section III. In Section IV, a Kalman filter for roll state estimation is designed and response characteristics of a lateral acceleration sensor and MSHub units are discussed. In Section V, the experimental electric vehicle is introduced. In addition, the estimation results obtained from field tests are illustrated to validate and evaluate the estimation performance of a proposed Kalman filter. Finally, summary and conclusion are given in Section VI.

II. Vehicle Dynamics for Estimator Design

In this section, a three degree-of-freedom (3–DOF) yaw plane model is introduced to describe the lateral motion of electric vehicles. The yaw plane representation is shown in Fig. 1.

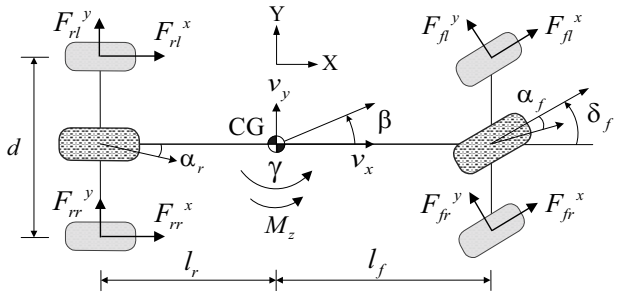

Fig. 1. 3–DOF yaw plane vehicle model.

The governing equations for longitudinal and lateral motions are given by

$$ma_x = F_r^x + F_f^x \cos\delta_f - F_f^y \sin\delta_f \quad (1)$$

$$ma_y = F_r^y + F_f^x \sin\delta_f + F_f^y \cos\delta_f \quad (2)$$

where the steering angles of front left and right wheels are assumed to be the same (i.e., = δ_f), front longitudinal tire force F_f^x is the sum of the front left and right longitudinal tire forces (i.e., $F_f^x = F_{fl}^x + F_{fr}^x$), rear longitudinal tire force F_r^x is the sum of the rear left and right longitudinal tire forces (i.e., $F_r^x = F_{rl}^x + F_{rr}^x$), front lateral tire force F_f^y is the sum of the front left and right lateral tire forces (i.e., $F_f^y = F_{fl}^y + F_{fr}^y$), and rear lateral tire force F_r^y is the sum of the rear left and right lateral tire forces (i.e., $F_r^y = F_{rl}^y + F_{rr}^y$).

The yaw moment balance equation with respect to point CG is

$$I_z\dot{\gamma} = l_f F_f^x \sin\delta_f + l_f F_f^y \cos\delta_f - l_r F_r^y + M_z \quad (3)$$

where the yaw moment, M_z, indicates a direct yaw moment control input, which is generated by the independent torque control of in-wheel motors. During yaw motion control, M_z is the control law to stabilize the vehicle motion and play a role as an additional input to the vehicle. Therefore, M_z is included in yaw moment balance equation and can be calculated as follows:

$$M_z = \frac{d}{2}(F_{rr}^x - F_{rl}^x) + \frac{d}{2}(F_{fr}^x - F_{fl}^x)\cos\delta_f. \quad (4)$$

Here, longitudinal tire forces can be obtained from a driving force observer which is designed based on wheel dynamics [32].

The tire slip angles are calculated based on geometric derivation using wheel velocity vectors. If the velocities at wheel ground contact points are known, the tire slip angles can be easily derived geometrically and are given by [33]

$$\alpha_{fl} = -\delta_f + \tan^{-1}\left(\frac{v_y + \gamma l_f}{v_x - \gamma d/2}\right) \quad (5)$$

$$\alpha_{fr} = -\delta_f + \tan^{-1}\left(\frac{v_y + \gamma l_f}{v_x + \gamma d/2}\right) \quad (6)$$

$$\alpha_{rl} = \tan^{-1}\left(\frac{v_y - \gamma l_r}{v_x - \gamma d/2}\right) \quad (7)$$

$$\alpha_{rr} = \tan^{-1}\left(\frac{v_y - \gamma l_r}{v_x + \gamma d/2}\right). \quad (8)$$

For design simplicity, the single track vehicle model (also called the bicycle model) is usually used in estimator design. By assuming that δ_f is relatively small, the lateral and yaw rate dynamics including a yaw moment control input are obtained as follows [17]:

$$ma_y = mv_x(\dot{\beta}+\gamma) = F_f^y + F_r^y \quad (9)$$

$$I_z\dot{\gamma} = l_f F_f^y - l_r F_r^y + M_z. \quad (10)$$

For small tire slip angles, the lateral tire forces can be linearly approximated as follows:

$$F_f^y = -2C_f\alpha_f = -2C_f\left(\beta + \frac{\gamma l_f}{v_x} - \delta_f\right) \quad (11)$$

$$F_r^y = -2C_r\alpha_r = -2C_r\left(\beta - \frac{\gamma l_r}{v_x}\right). \quad (12)$$

III. Design of Robust Sideslip Angle Estimator

The vehicle sideslip angle is defined as the angle between the longitudinal axis of the vehicle and the orientation of vehicle velocity vector [33]. The vehicle sideslip angle, shown in Fig. 2, is obtained as

$$\beta = \tan^{-1}\left(\frac{v_y}{v_x}\right). \quad (13)$$

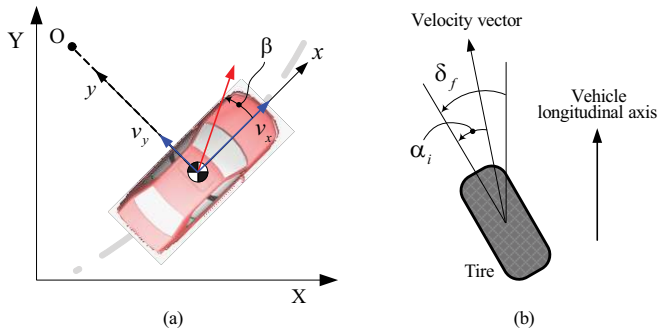

Fig. 2. Vehicle coordinates and tire slip angle: (a) Body fixed to global coordinates. (b) Tire slip angle.

A. Review on Conventional Sideslip Angle Estimation Methods

The conventional estimation methods of sideslip angle were proposed based on model-based observer design and direct sensor integration [11]. The model-based estimation method has the advantages of high accuracy in linear tire region and robustness against sensor bias. However, the estimation accuracy is dominantly dependent on vehicle parameters, tire parameters, and driving conditions. Since it is difficult to correctly identify the vehicle parameters (e.g., mass) and tire parameters (e.g., tire cornering stiffness) in real-time, a model-based estimation method can not provide reliable estimation over all driving conditions.

In the model-based estimation method, a linear bicycle model is used for estimator design. Based on a linear bicycle model and a linear tire model, state observers and Kalman filter were mainly used for sideslip angle estimation [15], [16]. Based on state space equations obtained from (9)–(12), a state observer is designed as follows:

$$\begin{aligned}\dot{\hat{x}} &= A_b\hat{x} + B_b u + L(y-\hat{y}) \\ \hat{y} &= C_b\hat{x}\end{aligned} \quad (14)$$

where $\hat{x} = [\hat{\beta}_{mod} \;\; \hat{\gamma}]^T$, $u = [\delta_f \;\; M_z]^T$, and $y = \gamma$

$$A_b = \begin{bmatrix} \frac{-2(C_f+C_r)}{mv_x} & \frac{-2(l_fC_f - l_rC_r)}{mv_x^2} - 1 \\ \frac{-2(l_fC_f - l_rC_r)}{I_z} & \frac{-2(l_f^2C_f + l_r^2C_r)}{I_z v_x} \end{bmatrix}$$

$$B_b = \begin{bmatrix} \frac{2C_f}{mv_x} & 0 \\ \frac{2l_fC_f}{I_z} & \frac{1}{I_z} \end{bmatrix}, \quad C_b = \begin{bmatrix} 0 & 1 \end{bmatrix}.$$

From the above state observer, the model-based sideslip angle estimate, $\hat{\beta}_{mod}$, is obtained. The critical aspect of this approach is that estimation performance dominantly relies on the tire model and variations in vehicle parameters. In order to minimize the effects of model mismatch, several researchers have proposed estimation methods for cornering stiffness, which is dependent on tire-road friction coefficients. In [17], a novel linear observer that uses a lateral acceleration sensor and yaw rate sensor as sensor measurements was proposed, and a fuzzy rule-based observer was also designed in order to cope with nonlinearities in vehicle models.

The sensor kinematics-based estimation method is based on the kinematic relationship among sensor measurements [11]. The equation of sensor kinematics is expressed as

$$\dot{\hat{\beta}}_{kin} = \frac{a_{ym} - g\phi}{v_x} - \gamma. \quad (15)$$

In order to obtain sideslip angle from (15), a direct numerical integration of (15) is required, but this causes a signal drift problem due to sensor bias. Moreover, since the lateral acceleration measurement contains a gravity effect caused by roll motion, the gravity effect should be compensated for accurate estimation (e.g., over-estimation is avoided by compensating the gravity effect). In practice, the numerical integration with a suitable forgetting factor is carried out to avoid severe signal drift.

In [11] and [13], the combined method of model-based estimation and kinematics-based estimation was proposed to make use of advantages of the two estimation methods. The model-based estimate is used at low frequencies (i.e., with low pass filter) while the kinematics-based estimate is used at higher frequencies (i.e., with high pass filter). The estimated sideslip angle from the combined estimation method was expressed as [11]

$$\begin{aligned}\hat{\beta}_{com} &= \frac{1}{1+\tau s}\hat{\beta}_{mod} + \frac{\tau}{1+\tau s}\dot{\hat{\beta}}_{kin} \\ &= \frac{1}{1+\tau s}\hat{\beta}_{mod} + \frac{\tau s}{1+\tau s}\hat{\beta}_{kin}.\end{aligned} \quad (16)$$

Here, the parameter, τ, is utilized for the filter setting.

B. Proposed Sideslip Angle Estimation Method

A novel method to estimate vehicle sideslip angle is proposed based on lateral vehicle velocity estimation. The proposed method uses the lateral tire forces which can be measured from MSHub units. Note that if the vehicle longitudinal and lateral velocities are obtained, the vehicle sideslip angle can be easily calculated. The lateral vehicle velocity is estimated using a RLS algorithm and its estimate is used to finally calculate the vehicle sideslip angle. In order to design a lateral vehicle velocity estimator, a simplified lateral tire force model (i.e., neglecting longitudinal tire force effects, see [33]) is used.

$$F_i^y = -C_i \tan(\alpha_i). \tag{17}$$

The above simplified lateral tire force model is applied to front left and right tires, respectively. For purposes of lateral vehicle velocity estimation, lateral tire force models for front tires are utilized based on following assumptions.

1) The left and right tires have pure tire slip conditions with negligible longitudinal slip and the peak lateral tire force occurs at the same tire slip angle. Tire slip angles, where the peak lateral tire forces occur at, are affected by weight transfer of vehicles. In contrast to engine vehicles, in-wheel-motor-driven electric vehicles, having battery packs under the floor and driving motors attached in wheels, can lower a CG of the vehicle. This provides the less weight transfer and thereby improves the driving stability. From these features, variations in front left and right tire forces due to weight transfer are not considered.
2) Front left and right tire cornering stiffnesses are the same (i.e., C_{fl}=C_{fr}≈C_f). Considering that front tires are on the same road surface and effects of weight transfer are not critical, effects of weight transfer in tire cornering stiffnesses of left and right tires are not considered.
3) From small angle approximations, $\tan(\alpha_i) \approx \alpha_i$.

From the above assumptions, front lateral tire forces can be expressed as

$$F_{fl}^y = -C_{fl}\alpha_{fl} \approx -C_f\left(\frac{v_y+\gamma l_f}{v_x-\gamma d/2}-\delta_f\right) \tag{18}$$

$$F_{fr}^y = -C_{fr}\alpha_{fr} \approx -C_f\left(\frac{v_y+\gamma l_f}{v_x+\gamma d/2}-\delta_f\right). \tag{19}$$

By dividing (18) by (19), the lateral vehicle velocity v_y is derived as

$$v_y = \gamma l_f - \frac{\delta_f(F_{fl}^y - F_{fr}^y)}{\dfrac{F_{fl}^y}{v_x+\gamma d/2} - \dfrac{F_{fr}^y}{v_x-\gamma d/2}} \tag{20}$$

where the estimated lateral vehicle velocity is defined as a pseudo-measurement and expressed as $\tilde{v}_y$. As described in (20), the proposed estimation method makes use of the ratio of front left and right lateral tire forces and is based on linearized tire models of front left and right tires by above assumptions. Even though we use linearized tire models in estimator design, the proposed estimator shows better estimation results with relatively small errors compared with results of conventionally used methods, even when lateral tire forces reach a peak value (e.g., up to 5m/s^2 of lateral acceleration, see Fig. 3(b)). We can confirm that a proposed estimator is robust against road conditions without using complicated nonlinear tire models only if front tires are on the same road surface. In section IV, this pseudo-measurement $\tilde{v}_y$ is used as a sensor measurement in the roll angle estimator using a Kalman filter.

Considering that all output data and input data are determined at sample instant, v_y described in (20) can thus be formulated by the RLS algorithm.

$$y(t) = \varphi^T(t)\theta(t) \tag{21}$$

where the estimated parameter $\theta(t)$, input regression $\varphi^T(t)$, and measured output $y(t)$ are given as

$$\theta(t) = \tilde{v}_y$$
$$\varphi^T(t) = \left(\frac{F_{fl}^y}{v_x+\gamma d/2} - \frac{F_{fr}^y}{v_x-\gamma d/2}\right)$$
$$y(t) = \gamma l_f\left(\frac{F_{fl}^y}{v_x+\gamma d/2} - \frac{F_{fr}^y}{v_x-\gamma d/2}\right) - \delta_f(F_{fl}^y - F_{fr}^y).$$

The ultimate goal of the RLS algorithm is to provide parameter estimates that minimize the following weighted least squares criterion [34]:

$$\hat{\theta}(t) = \arg\min_{\theta}\left\{\sum_{k=1}^{t}\Gamma(t,k)\cdot\rho[\varepsilon(k|\theta)]\right\}. \tag{22}$$

Here, $\Gamma(t,k)$ is the weight on the prediction errors at time k, and $\rho(\varepsilon)$ is the cost function which is defined as $\rho(\varepsilon) = \frac{1}{2}\varepsilon^2$. If the prediction errors can be assumed to be Gaussian with zero mean values, the defined cost function is reasonable.

The recursive process of the RLS algorithm, in a Kalman filter interpretation, is described as

$$\begin{aligned}
\hat{\theta}(t) &= \hat{\theta}(t-1) + K(t)\cdot\varepsilon\Big(t|\hat{\theta}(t-1)\Big)\\
\varepsilon\Big(t|\hat{\theta}(t-1)\Big) &= y(t) - \hat{y}\Big(t|\hat{\theta}(t-1)\Big)\\
&= y(t) - \varphi^T(t)\cdot\hat{\theta}(t-1)\\
K(t) &= P(t-1)\varphi(t)[\lambda I + \varphi^T(t)P(t-1)\varphi(t)]^{-1}\\
P(t) &= \frac{1}{\lambda}[I - K(t)\varphi^T(t)]P(t-1)
\end{aligned} \tag{23}$$

where I is the identity matrix, $\varepsilon(t)$ is the prediction error, and $K(t)$ and $P(t)$ are the Kalman gain and covariance matrices.

In order to cope with time-varying properties in a vehicle system, the weighted least squares criterion (22) is handled by putting less weight on older measurements. Therefore, the weighting function is set to [34]

$$\Gamma(t,k) = \lambda^{t-k} \tag{24}$$

where the forgetting factor, λ, is always chosen to be a positive constant slightly smaller than 1. The smaller λ is, the less weight is assigned to the older data; that is, the past data are forgotten faster. In this paper, λ around 0.995 was selected to make reasonable trade-off between tracking ability and noise sensitivity. From the RLS algorithm (23), the lateral vehicle

velocity is estimated and used to calculate the vehicle sideslip angle. The sideslip angle is easily calculated by (13) with vehicle velocity and pseudo-measurement $\tilde{v}_y$. The average value of the non-driven wheel velocities is used as a vehicle velocity. Considering that an electric vehicle used in field tests was a rear-wheel drive vehicle, it is reasonable to use non-driven wheel's velocity as a vehicle velocity. In case that the wheel slip occurs in non-driven wheels due to sudden braking, we can not use non-driven wheel's velocity for calculating the vehicle velocity. However, rear-wheel drive electric vehicles have Anti-lock Braking System (ABS), which contributes to keeping a vehicle steerable and stable during heavy braking moments by preventing wheel lock, for efficient braking of non-driven wheels and thereby severe wheel slip in non-driven wheels can be avoided.

Compared with the aforementioned conventional estimation methods, the main advantages of the proposed estimation method, utilizing lateral tire force sensors, are summarized in three points. First, it is robust against variations in vehicle parameters and tire-road conditions. Second, the proposed method can be easily realized without using additional sensors. Finally, the proposed recursive algorithm is very simple and can be easily implemented in real-time. Moreover, the estimated sideslip angle can be used to identify cornering stiffness in (18) and (19). The real-time information on cornering stiffness will contribute to improving the control performance of advanced motion control systems.

C. Experimental Results

The proposed estimation method was implemented on the experimental electric vehicle shown in Fig. 9. Moreover, to verify the effectiveness of the proposed method through comparison study, conventional estimation methods were also implemented and those results are evaluated by comparing the results of a proposed method. The specification and explanation for the experimental electric vehicle are introduced in section V.

In this study, a variety of field tests were performed with following driving conditions: 1) constant vehicle speed; 2) various steering commands, e.g., pulse steering, sine steering, and random steering; 3) without activation of vehicle motion controllers such as anti-slip control or yaw stability control (this means that the same current commands are applied to rear left and right in-wheel motors, i.e., control input M_z in (3) is equal to zero); 4) rear-wheel driving mode.

Experimental results obtained from a random steering test at v_x=40 km/h are shown in Fig. 3(a). Even though estimated sideslip angles obtained from model-based estimation method and combined method follow the measured sideslip angle, there still exist estimation errors due to model uncertainties in the observer model and numerical integration errors. On the other hand, the proposed estimation method shows more accurate estimation. In this result, the sensor measurement (i.e., thick gray line) is the actual value which is directly measured from the non-contact optical sensor. Fig. 3(b) and (c) show the results obtained from a pulse steering test and slalom test at v_x=50 km/h on wet asphalt, respectively. The

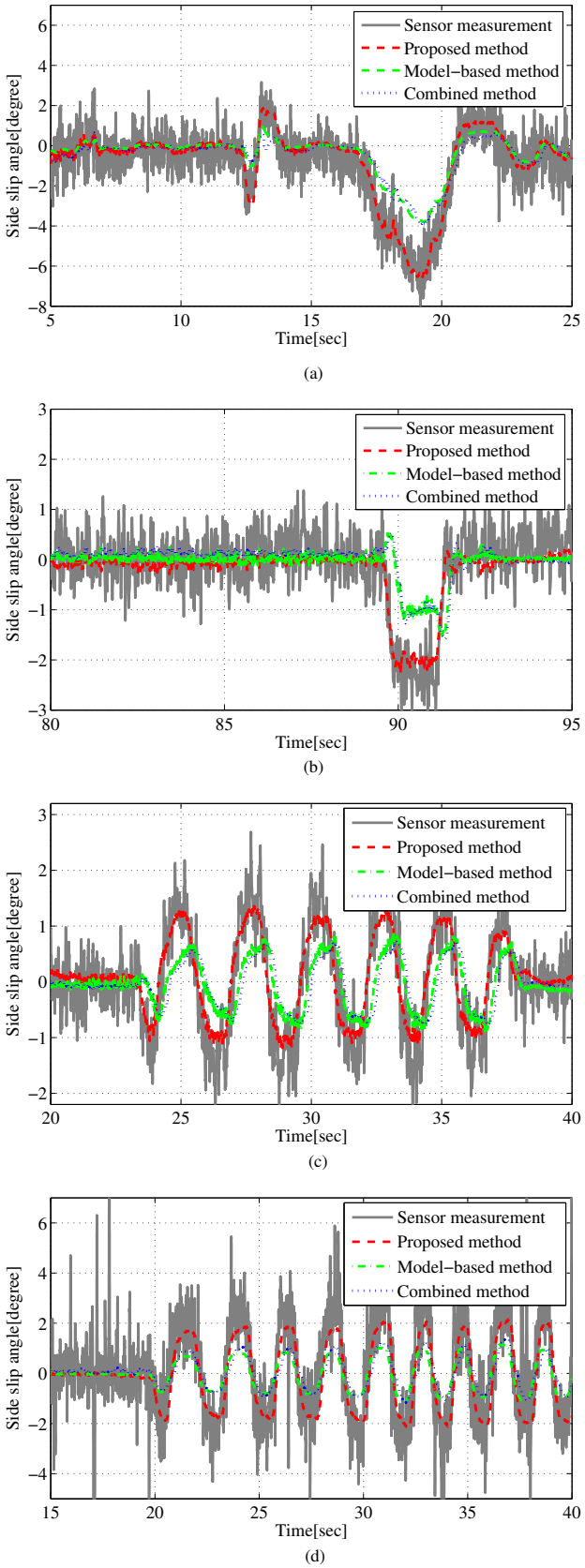

Fig. 3. Experimental results for the sideslip angle estimation: (a) Random steering test on dry asphalt (i.e., $\mu\simeq$0.9); maximum lateral acceleration 5 m/s^2. (b) Pulse steering test on wet asphalt (i.e., μ=0.7); maximum lateral acceleration 6 m/s^2. (c) Slalom test on wet asphalt (i.e., $\mu\simeq$0.7); maximum lateral acceleration 4 m/s^2. (d) Slalom test on a slippery road (i.e., $\mu\simeq$0.3); maximum lateral acceleration 2 m/s^2.

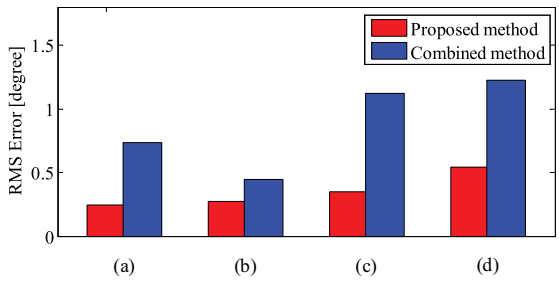

Fig. 4. Calculated RMS errors for estimation.

estimation results for two conventional methods contain errors with phase lag. The proposed estimation method provides very accurate estimation without any noticeable phase lag. To verify the robustness of the proposed estimation method, field tests on a slippery road (i.e., $\mu \simeq 0.3$) were also carried out and its result is shown in Fig. 3(d). Even though the results show larger estimation errors compared with the results on dry and wet asphalt, the estimation error was significantly decreased by applying the proposed method.

For quantitative evaluation of the proposed estimation method, the RMS values of estimation errors for different field tests were compared.

$$\text{RMS error} = \sqrt{\frac{1}{N}\sum_{j=1}^{N}(\hat{\beta}_j - \beta_{sensor,j})^2} \qquad (25)$$

where N is the number of samples. $\hat{\beta}_j$ and $\beta_{sensor,j}$ represent the estimated and measured sideslip angles at the jth sample. (a),(b),(c), and (d), seen in Fig. 4, correspond to the test results, shown in Fig. 3(a)–(d). As shown in Fig. 4, the proposed estimation method shows much smaller RMS values.

IV. Design of Roll Angle Estimator

Vehicle roll motion generally occurs as a result of lateral motion by steering maneuvers or road disturbances. In contrast to conventional engine vehicles, electric vehicles with in-wheel motors have a low ratio of sprung mass over unsprung mass due to having in-wheel motors installed in each wheel. This implies that ride quality can be deteriorated. In order to avoid deterioration in ride quality, the suspension stiffness was selected as a smaller value. It indicates that the roll motion easily occurs. Thus, a roll stability control system is required and an accurate roll angle should be obtained before control design. In this section, a roll angle estimation method, which uses sensor kinematic relationships and a linear roll model, is introduced. In a proposed roll angle estimator, lateral tire forces which are measured by MSHub units are utilized to estimate roll angle for the first time.

A. Roll Dynamics for Kalman Filter Design

This section introduces roll dynamics for Kalman filter design. Fig. 5 shows the two-dimensional roll dynamics for electric vehicles with in-wheel motors. In order to model the roll dynamics, the following assumptions are made:

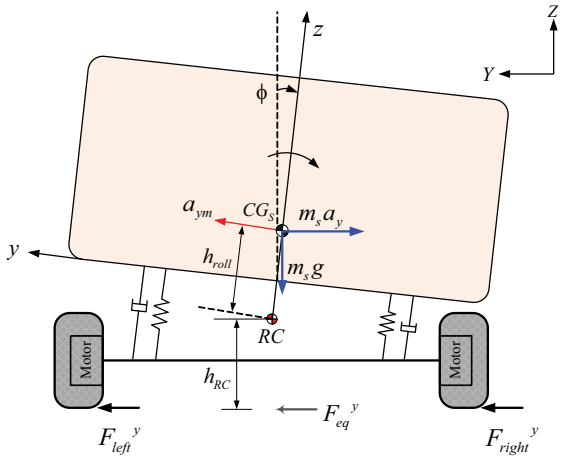

Fig. 5. 2–dimensional roll dynamics for an electric vehicle.

1) The location of the roll axis is constant with height h_{RC} and the lateral and vertical movements of RC due to the asymmetric suspension geometry are not considered.
2) Since roll angle is small, $\sin\phi \approx \phi$ and $\cos\phi \approx 1$.
3) Pitching and bouncing motion of sprung mass are neglected.
4) The effect of the road bank angle is not considered in this study.

The two-dimensional roll dynamic equation [24], the kinematic relationships of the lateral acceleration of CG, a_y, and sensor measurement, a_{ym}, are expressed as

$$\begin{aligned} I_x\ddot{\phi} + C_{roll}\dot{\phi} + K_{roll}\phi &= m_s(a_{ym})h_{roll} \\ &= m_s(a_y + g\phi)h_{roll} \qquad (26) \\ a_y &= \dot{v_y} + \gamma v_x \qquad (27) \\ a_{ym} &= \dot{v_y} + \gamma v_x + g\phi. \qquad (28) \end{aligned}$$

In (26), a roll moment acting on the sprung mass, which is caused by lateral motion, can be explained by lateral inertial force and gravity force of the sprung mass. The lateral acceleration effect in roll moment generation can be equivalently explained by lateral tire forces applied on tires, and the equivalent equation using lateral tire forces can be derived from the roll moment balance equation with respect to point RC as seen in Fig. 5.

$$\sum M_x = m_s(a_y + g\phi)h_{roll} = F_{eq}^y h_{RC}. \qquad (29)$$

Here, F_{eq}^y is the equivalent lateral tire force causing roll motion, which corresponds to roll motion caused by lateral acceleration of sprung mass. In (29), F_{eq}^y is replaced by lateral tire forces measured from the MSHub units, installed in each wheel. Therefore, an external roll moment acting on the sprung mass is explained with lateral tire forces.

$$F_{eq}^y h_{RC} \approx (F_{left}^y + F_{right}^y)h_{RC} = \sum_{i=1}^{4}(F_i^y)h_{RC}. \qquad (30)$$

Combining (26), (29), and (30), and using lateral tire forces as an external input, the following roll dynamics is obtained.

$$I_x\ddot{\phi} + C_{roll}\dot{\phi} + K_{roll}\phi = \sum_{i=1}^{4}(F_i^y)h_{RC}. \qquad (31)$$

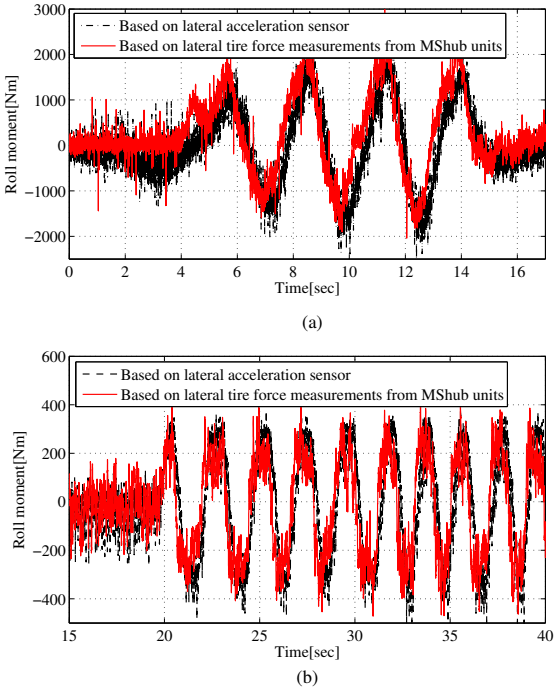

Fig. 6. Roll moment induced by the lateral vehicle motion: (a) Driving on dry asphalt ($\mu \simeq 0.9$). (b) Driving on a slippery road ($\mu \simeq 0.3$).

In contrast to conventional roll model-based estimation methods, the proposed roll angle estimation method uses lateral tire forces as inputs. Therefore, the effects of nonlinear tire characteristics (e.g., tire deflection by load transfer) can be considered in roll dynamics by directly using measured lateral tire forces. In this paper, two Kalman filters are designed–one that uses lateral tire force measurements ("Fy-based method"), and one that uses lateral acceleration measurements ("Ay-based method"). Since the MSHub units are superior to the lateral acceleration sensor in response time, it is expected that estimations based on lateral tire force measurements will lead that of estimations based on lateral acceleration measurements. Since the main source of lateral dynamic motion is the lateral tire force induced by driver's steering actions, the measured lateral tire forces can provide accurate estimation of vehicle states.

In order to check the response characteristics of two sensors (i.e., a lateral acceleration sensor and a MSHub unit), the roll moments, described in (29), were calculated from experiment data obtained in field tests on dry asphalt and a slippery road, respectively. From field test data, it is founded that the response time difference between a MSHub unit and a lateral acceleration sensor ranges from 80msec to 200msec. Fig. 6 shows the roll moments calculated from (29). As shown in Fig. 6, the roll moment calculated from lateral acceleration measurements has phase lag compared with the calculated roll moment from lateral tire force measurements.

B. Kalman Filter Design for Roll Angle Estimation

In this section, vehicle states are estimated using available sensor measurements and roll dynamics. The Kalman filter

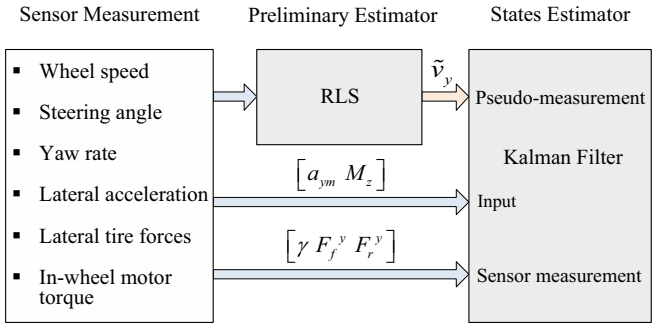

Fig. 7. Schematic of the roll angle estimator.

was applied to estimate unknown states (e.g., roll angle and roll rate) and to smoothen the sensor measurement noise. An overall structure of the proposed state estimator is shown in Fig. 7. The process of roll angle estimation can be divided into two stages: first, the preliminary estimation of a lateral vehicle velocity is conducted using the sensor measurements; second, this preliminary estimate (i.e., pseudo-measurement) and available sensor measurements are used in Kalman filter design for roll angle estimation. The estimated v_y from (20) is considered as a measurement variable, called a pseudo-measurement $\tilde{v}_y$, and thereby (28) can be rewritten as follows:

$$\dot{\tilde{v}}_y = a_{ym} - \gamma v_x - g\phi. \tag{32}$$

From (10), (31), and (32), the state space equation for Kalman filter design is obtained as

$$\begin{aligned} \dot{x} &= Ax + Bu + w \\ y &= Cx + v \end{aligned} \tag{33}$$

where A, B, and C are defined at the top of the next page. State variables, inputs, and measurement outputs are defined as

$$x = [\ \tilde{v}_y \quad \gamma \quad \phi \quad \dot{\phi} \quad F_f^y \quad F_r^y\ ]^T, \quad u = [\ a_{ym} \quad M_z\ ]^T,$$
$$y = [\ \tilde{v}_y \quad \gamma \quad F_f^y \quad F_r^y\ ]^T.$$

Note that the system described by (33) could be completely observable by using $\tilde{v}_y$ in (32) as a sensor measurement. Observability, which is concerned with the problem of determining the states of a dynamics system from observations of the output and control vectors, is examined through a rank condition on the Kalman observability matrix. By using pseudo-measurement $\tilde{v}_y$, (A, C) is observable (which means that observability matrix has full rank).

For real-time implementation, (33) is discretized as follows:

$$\begin{aligned} x[k+1] &= G[k]x[k] + H[k]u[k] + w[k] \\ y[k] &= C[k]x[k] + v[k] \end{aligned} \tag{34}$$

where

$$G[k] = e^{AT_s}, \quad H[k] = \int_0^{T_s} e^{A\tau} B d_\tau$$
$$C[k] = C, \quad T_s : \text{Sampling time.}$$

Here, $w[k]$ and $v[k]$ are the process noise and measurement noise, k is the time step. It is assumed that the process and

$$A=\begin{bmatrix} 0 & -v_x & -g & 0 & 0 & 0 \\ 0 & 0 & 0 & 0 & \frac{l_f}{I_z} & \frac{-l_r}{I_z} \\ 0 & 0 & 0 & 1 & 0 & 0 \\ 0 & 0 & -\frac{K_{roll}}{I_x} & -\frac{C_{roll}}{I_x} & \frac{h_{RC}}{I_x} & \frac{h_{RC}}{I_x} \\ 0 & 0 & 0 & 0 & 0 & 0 \\ 0 & 0 & 0 & 0 & 0 & 0 \end{bmatrix}, \quad B=\begin{bmatrix} 1 & 0 \\ 0 & \frac{1}{I_z} \\ 0 & 0 \\ 0 & 0 \\ 0 & 0 \\ 0 & 0 \end{bmatrix}, \quad C=\begin{bmatrix} 1 & 0 & 0 & 0 & 0 & 0 \\ 0 & 1 & 0 & 0 & 0 & 0 \\ 0 & 0 & 0 & 0 & 1 & 0 \\ 0 & 0 & 0 & 0 & 0 & 1 \end{bmatrix}$$

measurement noise are zero-mean Gaussian processes, and the covariance matrices are given as follows:

$$Q_w = E(w[k]w[k]^T) > 0 \tag{35}$$

$$R_v = E(v[k]v[k]^T) \gg 0 \tag{36}$$

$$E(w[k]v[k]^T) = 0. \tag{37}$$

The Kalman filter bandwidth and its susceptibility to sensor measurement noise totally depend on the process noise covariance matrix Q_w and the measurement noise covariance matrix R_v, which represent level of confidence placed in the accuracy of the observer model and sensor measurements. These matrices determine the filter characteristics including accuracy and response, and their matrix values were experimentally determined by using sensor measurements. In this paper, the covariance matrices of process noise and measurement noise are given as follows:

$$Q_w = \text{diag}[Q_{\tilde{v}_y}, Q_\gamma, Q_\phi, Q_{\dot{\phi}}, Q_{F_f^y}, Q_{F_r^y}] \tag{38}$$

$$R_v = \text{diag}[R_{\tilde{v}_y}, R_\gamma, R_{F_f^y}, R_{F_r^y}]. \tag{39}$$

In principle, the covariance matrices are not necessarily diagonal. However, treating the noise covariance matrix as a diagonal matrix (i.e., individual noise components are not cross-correlated) is advantageous since it reduces computation time. In selection of covariance matrices, it should be noted that the less noise in sensor measurements compared to the uncertainty in dynamics model, the more the states will be adapted to follow sensor measurements. Since the new measurements for lateral tire forces are much more accurate than the prior estimates, we put the high uncertainty on states (i.e., lateral tire forces). The states (e.g., roll angle and roll rate) are modeled using reliable vehicle roll dynamics. Therefore, the process noises are relatively small. The suitable process noise variances for other states (e.g., lateral vehicle velocity and yaw rate) are selected based on comparison to the corresponding measurement noise variances. The noise variances of three sensor measurements are determined from statistical data analysis (e.g., a statistical evaluation of the histogram) using Matlab software.

The Kalman filter, designed based on (33)–(39), performs filtering and prediction [35]. The basic steps of computational procedure for the Kalman filter are illustrated in Fig. 8.

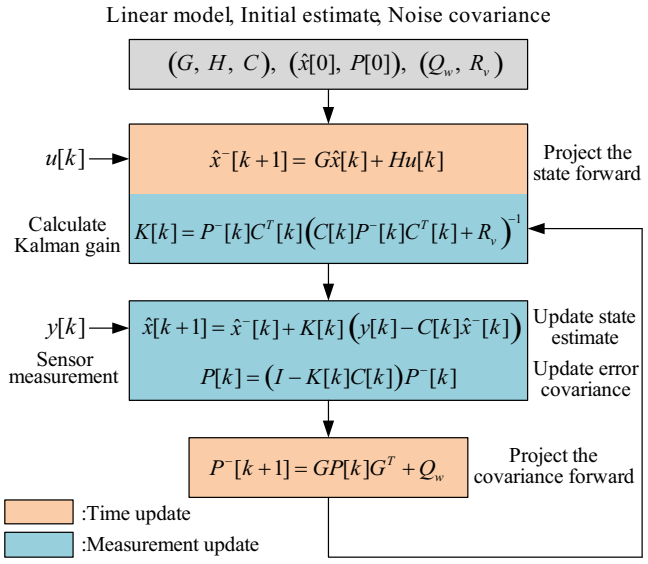

Fig. 8. Recursive structure of the Kalman filter algorithm.

V. Experimental Verification

The proposed estimation method was implemented on the experimental electric vehicle shown in Fig. 9. In order to evaluate estimation results of the Kalman filter, the vertical potentiometers and a roll rate sensor were used to accurately measure the roll angle and roll rate. The random steering test and pulse steering test on dry asphalt were conducted and field tests on wet asphalt and a slippery road were also carried out to verify the robustness against road conditions. Moreover, the same driving conditions, described in Section III. C, were applied in field tests.

A. Experimental Electric Vehicle: FPEV–II Kanon

The experimental electric vehicle named "FPEV–II Kanon", shown in Fig. 9, was used for field tests. The "FPEV–II Kanon" was developed by the Hori/Fujimoto research team and it has following special features.

1) In-wheel motors (i.e., Permanent magnet motors) are mounted in each wheel as shown in Fig. 11(a). Therefore, we can control each wheel torque completely and independently for vehicle motion control. Regenerative braking is also available. The specifications of "FPEV–II Kanon" are listed in Table I.
2) MSHub units for measuring lateral tire forces in real-time are installed in each wheel. Fig. 11(b) shows the MSHub unit invented by NSK Ltd. [36].
3) 4WS (4 Wheel Steering) control is possible through front and rear EPS (Electric Power Steering) systems.

As shown in Fig. 10, sensor outputs from the MSHub units, gyro sensor, and steering angle sensor are connected to

Fig. 9. Experimental electric vehicle: FPEV–II Kanon.

TABLE I
SPECIFICATIONS OF FPEV–II KANON

In-wheel motor	
Type	Direct drive outer rotor type
Maximum Torque	500Nm(Front*)/340Nm(Rear*)
Maximum Power	20.0kW(Front*)/10.7kW(Rear*)
Weight	32kg(Front*)/26kg(Rear*)
Battery	
Type	Lithium-ion type
Capacity	5kWh
Numbers	10 modules (1module=4cell)
Control system	
Controller	AutoBox-DS1103
Sampling Time	0.001sec
Sensors	Gyro sensor, Wheel speed sensor, Steering angle sensor, Multi-sensing hub unit

Front*: one front wheel motor, Rear*: one rear wheel motor

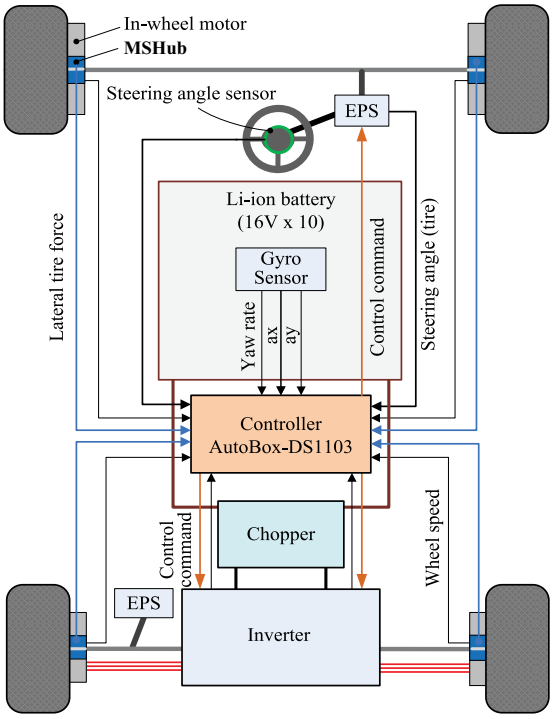

Fig. 10. Schematic of the electrical system of FPEV–II Kanon.

(a) (b)

Fig. 11. (a) Rear In-wheel motor, (b) Multi-sensing hub (MSHub) unit.

dSPACE AutoBox (DS1103), used for real-time data acquisition. The dSPACE AutoBox (DS1103), which is a powerful controller board for rapid control prototyping, consists of a power PC 750GX controller board running at 933 MHz, 16 channel A/D converter and 8 channel D/A converter. Additionally, a non-contact optical sensor, Correvit (Corrsys–Datron), is used for accurate measurements of sideslip angle, lateral vehicle velocity and longitudinal vehicle velocity, and its outputs are connected to AutoBox. The Correvit sensor uses optical means to capture planar road texture and evaluate the motion of the vehicle by measuring the direction and magnitude of change with respect to the road texture. The sensor outputs from vertical potentiometers and a roll rate sensor are also connected. The sampling time is set at 1ms.

Contrary to other experimental electric vehicles, the electric vehicle used in this research provides lateral tire forces in real-time. By directly using lateral tire forces, we can accurately estimate vehicle states. In addition, the heuristic tire models are not required in estimator and control design. MSHub units, including rolling bearings used to support wheels of the vehicle, can measure the loads applied to the rolling bearing. In many conventional vehicles, wheel hub units with built-in active ABS sensors (i.e., wheel velocity sensor) were equipped. Comparing MSHub units with wheel hub units which are currently used in vehicles, MSHub units have almost the same mechanical structure except for rolling elements in a pair of rows and is capable of being constructed at a low cost. The measurement principle is as follows: the revolution speeds of rolling elements in a pair of rows are sensed by a pair of revolution speed sensors and difference of sensed revolution speeds is used to calculate the radial or axial loads [36]. Therefore, accurate lateral tire force measurements using MSHub units can be realized without much additional cost and, due to cost-effective aspects, MSHub units are recently considered practically applicable to vehicles by automotive manufacturers.

B. Experimental Results

Experimental results obtained from field tests are presented to validate the estimator and to compare the Fy-based method and Ay-based method. Fig. 12 shows experimental results for the random steering test on dry asphalt. Driving conditions including vehicle speed and steering angle (i.e., wheel angle) are illustrated in Fig. 12(a). Fig. 12(b)–(d) present estimates of yaw rate, roll angle, and roll rate compared with sensor

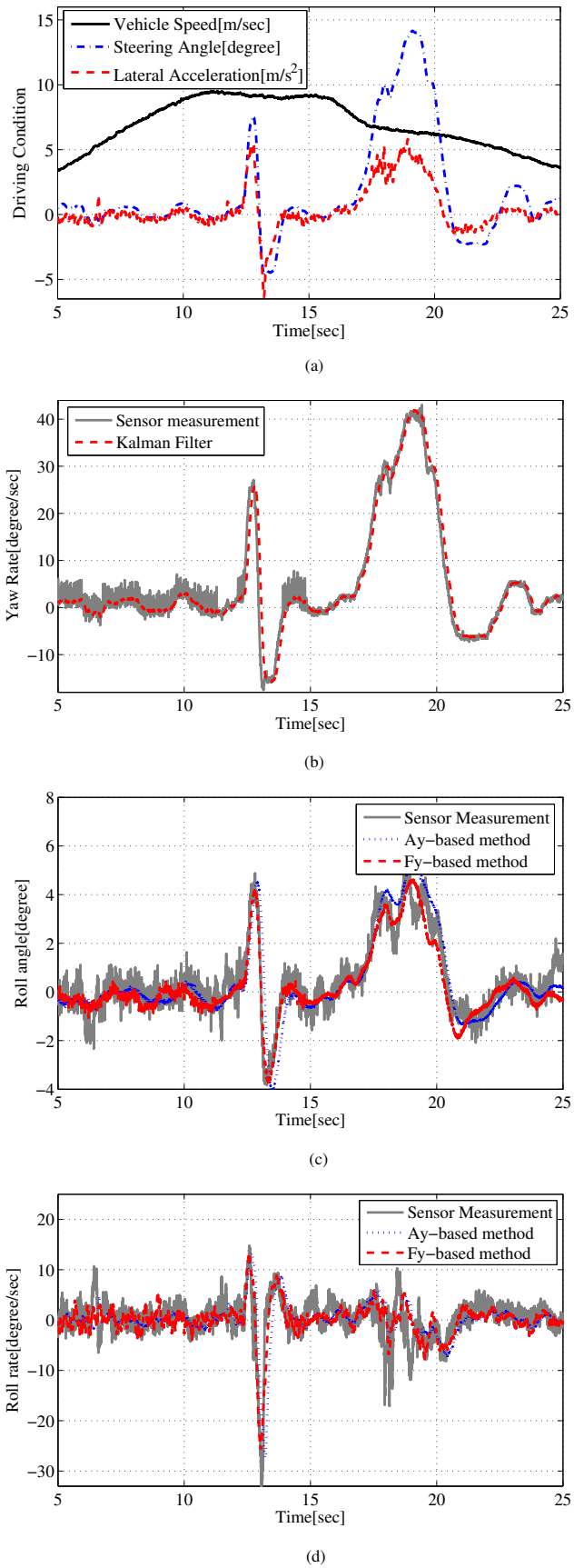

Fig. 12. Experimental results for roll state estimation in a random steering test on dry asphalt (i.e., $\mu \simeq 0.9$): (a) Driving condition. (b) Yaw rate. (c) Roll angle. (d) Roll rate.

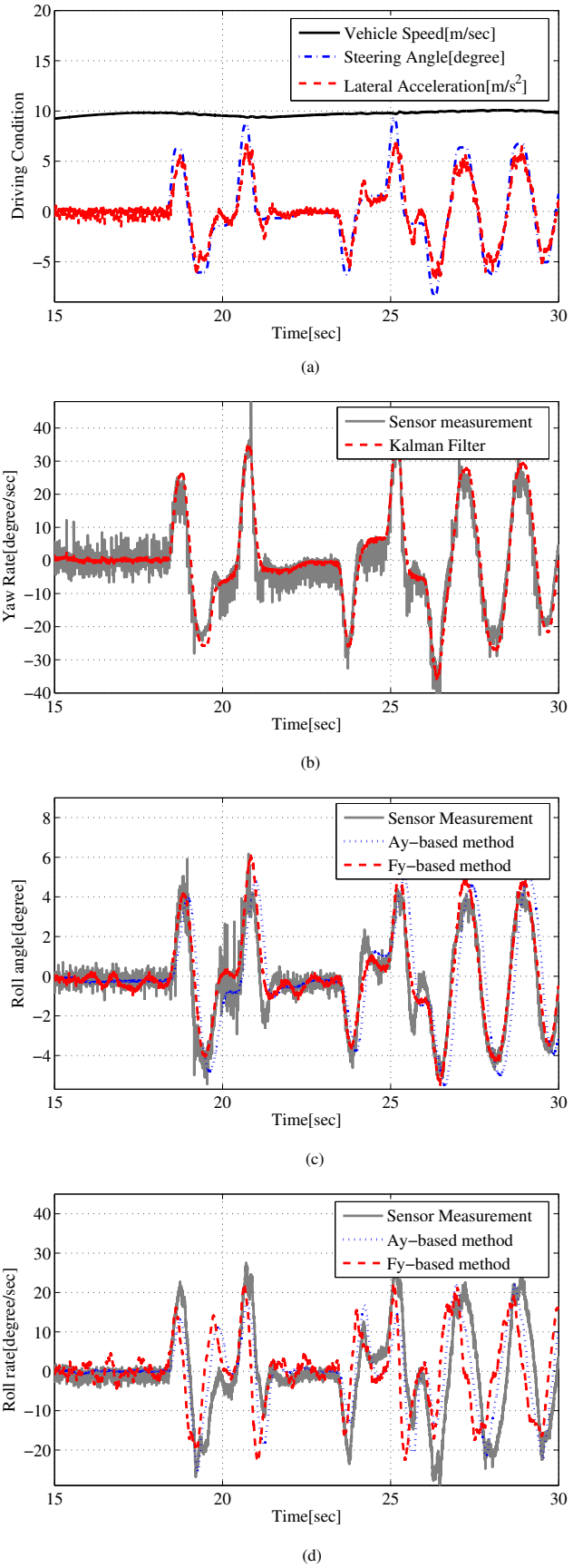

Fig. 13. Experimental results for roll state estimation in a random steering test on wet asphalt (i.e., $\mu \simeq 0.7$): (a) Driving condition. (b) Yaw rate. (c) Roll angle. (d) Roll rate.

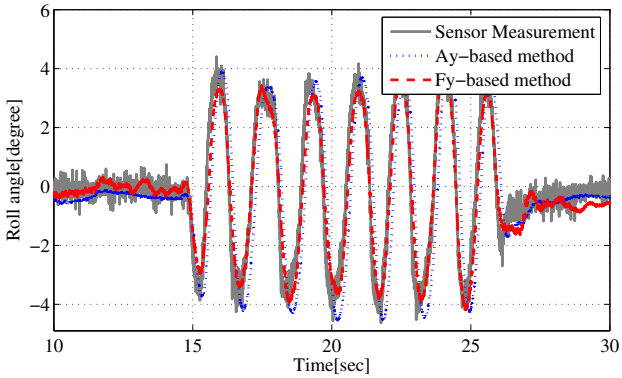

(a)

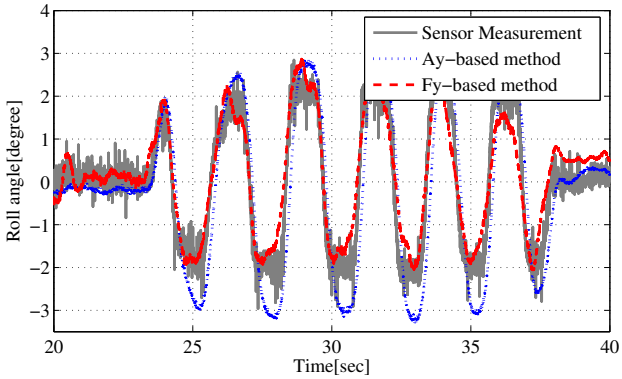

(b)

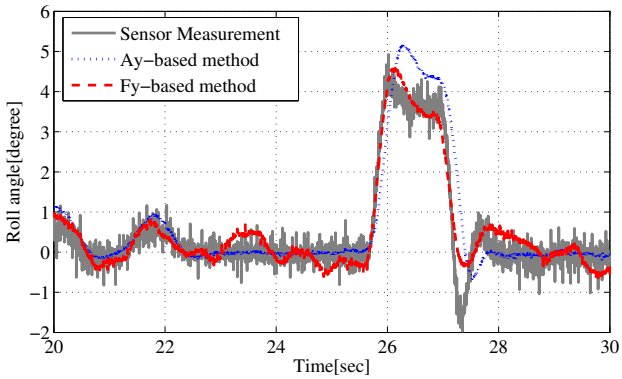

(c)

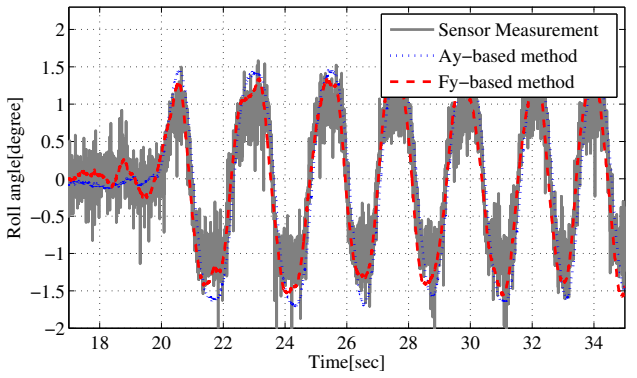

(d)

Fig. 14. Experimental results for roll angle estimation: (a) Driving at v_x=50 km/h on dry asphalt (i.e., $\mu\simeq$0.9). (b) Driving at v_x=40 km/h on dry asphalt (i.e., $\mu\simeq$0.9). (c) Driving at v_x=40 km/h on wet asphalt (i.e., $\mu\simeq$0.7). (d) Driving at v_x=30 km/h on a slippery road (i.e., $\mu\simeq$0.3).

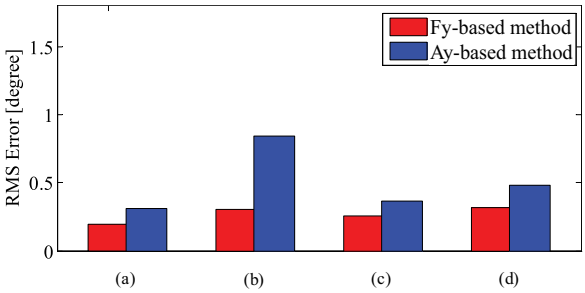

Fig. 15. Calculated RMS errors for estimation.

measurements. It can be seen that the estimated roll angle and roll rate track the sensor measurement values with small errors.

Experimental results obtained from the Fy-based and Ay-based methods are compared using Fig. 12(c) and (d). We can confirm that the Fy-based method shows more accurate results without noticeable phase lag. This agrees with earlier discussion about roll moments, which are calculated from lateral tire forces and lateral acceleration respectively. Fig. 13 shows experimental results of the random steering test at v_x=40 km/h on wet asphalt. Similarly, the proposed Kalman filter in this case provides accurate estimation with no phase lag.

In order to verify the robustness of the proposed Kalman filter, several field tests on different roads were performed and those results are shown in Fig. 14. The RMS values of estimation errors are shown in Fig. 15. The experimental results shown in Fig. 14(a)–(d) correspond to (a)–(d) in Fig. 15, and are explained as follows: (a) shows the result of a sine steering test at v_x=50 km/h on dry asphalt. As shown in Fig. 15, the roll angle estimated by the Kalman filter using lateral tire forces shows relatively low RMS values (in this case, the maximum roll angle is $|\phi|_{max}\approx$ 4 degree). (b) and (c) show the results of sine steering and pulse steering tests at v_x=40 km/h on dry asphalt and wet asphalt respectively. Roll angles estimated with the proposed Kalman filter track the measured values with small errors. It is noted that result (d), obtained from the field test on a slippery road, also shows the low RMS value. This implies that the proposed Kalman filter is robust to road conditions.

VI. Conclusion

This paper presents novel estimation methods to accurately estimate the vehicle sideslip angle and roll angle using lateral tire force sensors. The RLS algorithm and a Kalman filter were used in estimator design. Characteristics of the proposed estimation methods, such as estimation performance and robustness, were discussed and evaluated through field tests under different road conditions. It was shown that the estimation methods utilizing lateral tire forces provide even more improved estimation of the vehicle sideslip angle and roll angle. Additionally, the experimental results demonstrated that Kalman filter design using lateral tire forces could provide reliable estimation without noticeable phase lag. By using

lateral tire force measurements, important vehicle states for vehicle stability control could be estimated without using expensive sensors and we could confirm the possibilities of the practical applications of MSHub units to vehicle stability control systems for in-wheel-motor-driven electric vehicles. This is one of the important results of this paper. From experimental results of proposed estimators, it is anticipated that lateral tire forces, measured from MSHub units, will provide practical solutions to challenging issues in vehicle state estimation. Since the proposed estimator for sideslip angle estimation is designed based on linear tire models, some estimation errors may occur during severe driving on low friction roads. Therefore, in future works, we will improve the tire model by taking into account nonlinear tire characteristics and an effect of road-bank angle. Moreover, advanced motion control systems based on proposed estimators will be presented.

APPENDIX

NOMENCLATURE

a_x	Longitudinal acceleration at center of gravity (CG) (m/s^2).
a_y	Lateral acceleration at CG (m/s^2).
a_{ym}	Sensor measurement of lateral acceleration (m/s^2).
d	Track width = 1.3 m.
g	Acceleration due to gravity = 9.81 m/s^2.
h_{roll}	Height of the center of sprung mass above roll center (RC) = 0.32 m.
h_{RC}	Height of the RC above the ground = 0.21 m.
i	1, 2, 3, 4 corresponding to front left, front right, rear left, and rear right (= fl, fr, rl, rr).
l_f	Distance from CG to front axle = 1.013 m.
l_r	Distance from CG to rear axle = 0.702 m.
v_x	Longitudinal velocity at CG of vehicle (m/s).
v_y	Lateral velocity at CG of vehicle (m/s).
$\tilde{v}_y$	Estimated lateral vehicle velocity (m/s).
m	Total mass of vehicle = 875 kg.
m_s	Sprung mass = 670 kg.
C_i	Tire cornering stiffness at the ith tire (N/rad).
C_f	Front tire cornering stiffness = 11200 N/rad.
C_r	Rear tire cornering stiffness = 31600 N/rad.
C_{roll}	Roll damping coefficient = 3200 N·m·s/rad.
F_i^x	Longitudinal tire force at the ith tire (N).
F_i^y	Lateral tire force at the ith tire (N).
F_{left}^y	Lateral tire force on the left track wheels (=F_{fl}^y+F_{rl}^y) (N).
F_{right}^y	Lateral tire force on the right track wheels (=F_{fr}^y+F_{rr}^y) (N).
I_x	Roll moment of inertia = 250 kg·m^2.
I_z	Yaw moment of inertia = 617 kg·m^2.
K_{roll}	Roll stiffness coefficient = 12000 N·m/rad.
L	Observer gain matrix.
M_x	Roll moment (N·m).
M_z	Yaw moment (N·m).
α_i	Slip angle at the ith tire (rad).
α_f	Front tire slip angle (rad).
α_r	Rear tire slip angle (rad).
β	Vehicle sideslip angle (rad).
$\hat{\beta}_{com}$	Estimated sideslip angle from combined method (rad).
$\hat{\beta}_{kin}$	Estimated sideslip angle from kinematics-based estimation method (rad).
$\hat{\beta}_{mod}$	Estimated sideslip angle from model-based estimation method (rad).
δ_f	Front steering angle (rad).
ϕ	Roll angle (rad).
$\dot{\phi}$	Roll rate (rad/s).
$\ddot{\phi}$	Roll acceleration (rad/s^2).
γ	Yaw rate (rad/s).
λ	Forgetting factor in RLS algorithm.
μ	Road friction coefficient.

ACKNOWLEDGMENT

The authors would like to thank NSK Ltd. for providing MSHub units and technical support.

REFERENCES

[1] Y. Hori, "Future vehicle driven by electricity and control-research on four-wheel-motored "UOT Electric March II"," *IEEE Trans. Ind. Electron.*, vol. 51, no. 5, pp. 654–962, Oct. 2004.

[2] S. Sakai, H. Sado, and Y. Hori, "Motion control in an electric vehicle with four independently driven in-wheel motors," *IEEE/ASME Trans. Mechatron.*, vol. 4, no. 1, pp. 9–16, Mar. 1999.

[3] D. Yin, S. Oh, and Y. Hori, "A novel traction control for EV based on maximum transmissible torque estimation," *IEEE Trans. Ind. Electron.*, vol. 56, no. 6, pp. 2086–2094, Jun. 2009.

[4] N. Mutoh and Y. Nakano, ''Dynamics of front-and-rear-wheel-independent-drive-type electric vehicles at the time of failure," *IEEE Trans. Ind. Electron.*, vol. 59, no. 3, pp. 1488–1499, Mar. 2012.

[5] Y. Chen and J. Wang, ''Fast and global optimal energy-efficient control allocation with applications to over-actuated electric ground vehicles," *IEEE Trans. Control Syst. Technol.*, vol. PP, no. 99, pp. 1–10, 2012.

[6] R. Wang and J. Wang, ''Fault-tolerant control with active fault diagnosis for four-wheel independently-driven electric ground vehicles," *IEEE Trans. Veh. Technol.*, Vol. 60, No. 9, pp. 4276–4287, Nov. 2011.

[7] H. Fujimoto, A. Tsumasaka, and T. Noguchi, ''Direct yaw-moment control of electric vehicle based on cornering stiffness estimation," in *Proc. of IEEE IECON*, Nov. 2005.

[8] K. Kawashima, T. Uchida, and Y. Hori, ''Rolling stability control of in-wheel electric vehicle based on two-degree-of-freedom control," in *Proc. of IEEE Advanced Motion Control*, Mar. 2008, pp. 751–756.

[9] H. E. Tseng, D. Madau, B. Ashrafi, T. Brown, and D. Recker, ''Technical challenges in the development of vehicle stability control system," in *Proc. IEEE Int. Conf. Control Appl.*, Aug. 1999, pp. 1660–1666.

[10] D. Fukada, "Slip-angle estimation for vehicle stability control," *Veh. Syst. Dyn.*, vol. 32, no. 4, pp. 375–388, Mar. 1999.

[11] D. Piyabongkarn, R. Rajamani, J. Grogg, and J. Lew, ''Development and experimental evaluation of a slip angle estimator for vehicle stability control," *IEEE Trans. Control Syst. Technol.*, vol. 17, no. 1, pp. 78–88, Jan. 2009.

[12] G. Phanomchoeng, R. Rajamani, and D. Piyabongkarn, ''Nonlinear observer for bounded Jacobian systems, with applications to automotive slip angle estimation," *IEEE Trans. Autom. Control*, vol. 56, no. 5, pp. 1163–1170, May 2011.

[13] M. Doumiati, A. Victorino, A. Charara, and D. Lechner, ''A method to estimate the lateral tire force and the sideslip angle of a vehicle: Experimental validation," in *Proc. American Control Conf.*, Baltimore, MD, Jul. 2010, pp. 6936–6942.

[14] J. Stephant, A. Charara, and D. Meizel, ''Virtual sensor: application to vehicle sideslip angle and transversal forces," *IEEE Trans. Ind. Electron.*, vol. 51, no. 2, pp. 278–289, Apr. 2004.

[15] F. Chelli, E. Sabbioni, M. Pesce, and S. Melzi, "A methodology for vehicle sideslip angle identification: comparison with experimental data," *Veh. Syst. Dyn.*, vol. 45, no. 6, pp. 549–563, Jun. 2007.

[16] M. C. Best, T. J. Gordon, and P. J. Dixon, "An extended adaptive kalman filter for real-time state estimation of vehicle handling dynamics," *Veh. Syst. Dyn.*, vol. 34, no. 1, pp. 57–75, Jul. 2000.

[17] G. Cong, L. Mostefai, M. Denai, and Y. Hori, "Direct yaw-moment control of an in-wheel-motored electric vehicle based on body slip angle fuzzy observer," *IEEE Trans. Ind. Electron.*, vol. 56, no. 5, pp. 1411–1419, May 2009.
[18] M. Doumiati, A. C. Victorino, A. Charara, and D. Lechner, "Onboard real-time estimation of vehicle lateral tire–road forces and sideslip angle," *IEEE/ASME Trans. Mechatron.*, vol. 16, no. 4, pp. 601–614, Aug. 2011.
[19] J. Dakhlallah, N. Glaser, S. Mammar, and Y. Sebsadji, ''Tire-road forces estimation using extended Kalman filter and sideslip angle evaluation," in *Proc. American Control Conf.*, Seattle, WA, Jun. 2008, pp. 4597–4602.
[20] G. Xiaojie, Y. Zhuoping, N. Jens, and W. Jochen, "Sideslip angle estimation based on input-output linearisation with tire-road friction adaptation," *Veh. Syst. Dyn.*, vol. 48, no. 2, pp. 217–234, Feb. 2010.
[21] S. You, J. Hahn, and H. Lee, ''New adaptive approaches to real-time estimation of vehicle sideslip angle," *Control Engineering Practice*, vol. 17, no. 12, pp. 1367–1379, Dec. 2009.
[22] D. M. Bevly, J. C. Gerdes, and C. Wilson, "The use of GPS based velocity measurements for measurement of sideslip and wheel slip," *Veh. Syst. Dyn.*, vol. 38, no. 2, pp. 127–147, Feb. 2003.
[23] J. Park , J. Yoon , D. Kim, and K. Yi, ''Roll state estimator for rollover mitigation control," *Proc. Inst. Mech. Eng., Part D: J. Automobile Eng.,*, vol. 222, no. 2, pp. 1289–1311, 2008.
[24] J. Ryu, N. K. Moshchuk, and S. K. Chen, ''Vehicle state estimation for roll control system," in *Proc. American Control Conf.*, New York, NY, Jul. 2007, pp. 1618–1623.
[25] A. Hac, T. Brown, and J. Martens, "Detection of vehicle rollover," *SAE.*, Int., Warrendale, PA, 2004-01-1757, 2004.
[26] J. Ryu and J. C. Gerdes, "Integrating inertial sensors with GPS for vehicle dynamics control," *J. Dynam. Syst., Meas., Control.*, pp. 243–254, Jun. 2004.
[27] R. Daily and D. M. Bevly, ''The use of GPS for vehicle stability control systems," *IEEE Trans. Ind. Electron.*, vol. 51, no. 2, pp. 270–277, Apr. 2004.
[28] D. M. Bevly, J. Ryu, and J. C. Gerdes, "Integrating INS sensors with GPS measurements for continuous estimation of vehicle sideslip, roll, and tire cornering stiffness," *IEEE Trans. Intell. Transport. Syst.*, vol. 7, no. 4, pp. 483–493, Dec. 2006.
[29] C. Paleologu, J. Benesty, and S. Ciochina, "A robust variable forgetting factor recursive least-squares algorithm for system identification," *IEEE Signal Process. Lett.*, vol. 15, pp. 597–600, 2008.
[30] P. J. T, Venhovens and K. Nabb, "Vehicle dynamics estimation using kalman filters ," *Veh. Syst. Dyn.*, vol. 32, no. 2, pp. 171–184, Aug. 1999.
[31] G. Baffet, A. Charara, and G. Dherbomez, "An observer of tireroad forces and friction for active security vehicle systems," *IEEE/ASME Trans. Mechatron.*, vol. 12, no. 6, pp. 651–661, Dec. 2007.
[32] H. Sado, S. Sakai, and Y. Hori, ''Road condition estimation for traction control in electric vehicle," in *Proc. IEEE Int. Symp. Ind. Electron.(ISIE 99)* , Jul. 1999, pp. 973–978.
[33] R. Rajamani, *Vehicle Dynamics and Control*. New York: Springer-Verlag, 2005.
[34] L. Ljung, *System Identification: Theory for the User*. Englewood Cliffs, NJ: Prentice-Hall, 1987.
[35] A. Gleb, Ed, *Applied Optimal Estimation*. Cambridge, MA: MIT Press, 1974.
[36] T. Takizawa, T. Yanagisawa, K. Ono, and I. Sakatani, "Load measuring device for rolling bearing unit and load measuring rolling bearing unit," U.S. Patent 7 320 257, Jan. 22, 2008.

Kanghyun Nam (S'10) received the B.S.degree in mechanical engineering from Kyungpook National University, Daegu, Korea, in 2007 and the M.S.degree in mechanical engineering from Korea Advanced Institute of Science and Technology (KAIST), Daejeon, Korea, in 2009. During 2008 to 2009, he was a control engineer with Advanced Brake System R&D Center, MANDO Corp., Korea. He is currently working toward the Ph.D.degree in electrical engineering with The University of Tokyo. His research interests include vehicle dynamics and control, state estimation and motion control for electric vehicles, and robust control.

He is a member of the Society of Automotive Engineers of Japan and the Korean Society of Automotive Engineers.

Sehoon Oh (S'05−M'06) received the B.S., M.S., and Ph.D.degrees in electrical engineering from The University of Tokyo, Tokyo, Japan, in 1998, 2000, and 2005, respectively. He is currently a project research professor in the Department of Electrical Engineering, The University of Tokyo. His research fields include the development of human friendly motion control algorithms and assistive devices for people.

Dr. Oh is a member of the Institute of Electrical Engineers of Japan, the Society of Instrument and Control Engineers, and the Robotic Society of Japan.

Hiroshi Fujimoto (S'99−M'01) received the Ph.D. degree in the Department of Electrical Engineering from the University of Tokyo in 2001. In 2001, he joined the Department of Electrical Engineering, Nagaoka University of Technology, Niigata, Japan, as a research associate. From 2002 to 2003, he was a visiting scholar in the School of Mechanical Engineering, Purdue University, U.S.A. In 2004, he joined the Department of Electrical and Computer Engineering, Yokohama National University, Yokohama, Japan, as a lecturer and he became an associate professor in 2005. He is currently an associate professor of the University of Tokyo since 2010. He received the Best Paper Award from the IEEE Transaction On Industrial Electronics in 2001, Isao Takahashi Power Electronics Award in 2010, and Best Author Prize of SICE in 2010. His interests are in control engineering, motion control, nano-scale servo systems, electric vehicle control, and motor drive.

Dr. Fujimoto is a member of IEE of Japan, the Society of Instrument and Control Engineers, the Robotics Society of Japan, and the Society of Automotive Engineers of Japan.

Yoichi Hori (S'81−M'83−SM'00−F'05) received his B.S., M.S., and Ph.D. degrees in Electrical Engineering from the University of Tokyo, Tokyo, Japan, in 1978, 1980, and 1983, respectively. In 1983, he joined the Department of Electrical Engineering, The University of Tokyo, as a Research Associate. He later became an Assistant Professor, an Associate Professor, and, in 2000, a Professor at the same university. In 2002, he moved to the Institute of Industrial Science as a Professor in the Information and System Division, and in 2008, to the Department of Advanced Energy, Graduate School of Frontier Sciences, the University of Tokyo. From 1991-1992, he was a Visiting Researcher at the University of California at Berkeley. His research fields are control theory and its industrial applications to motion control, mechatronics, robotics, electric vehicles, etc.

Prof. Hori has been the Treasurer of the IEEE Japan Council and Tokyo Section since 2001. He is the winner of the Best Transactions Paper Award from the IEEE Transactions on Industrial Electronics in 1993 and 2001, of the 2000 Best Transactions Paper Award from the Institute of Electrical Engineers of Japan (IEEJ), and 2011 Achievement Award of IEE-Japan. He is an IEEE Fellow and an AdCom member of IES. He is also a member of the Society of Instrument and Control Engineers; Robotics Society of Japan; Japan Society of Mechanical Engineers; and the Society of Automotive Engineers of Japan. He was the President of the Industry Applications Society of the IEEJ, the President of Capacitors Forum, and the Chairman of Motor Technology Symposium of Japan Management Association (JMA) and the Director on Technological Development of SAE-Japan (JSAE).